Computational Analysis of Safety Injection Tank Performance

Jai Oan Cho[a], Yohanes Setiawan Nietiadi[a], Jeong Ik Lee[a]*, Yacine Addad[b], Ho Joon Yoon[b]
[a]*Department of Nuclear and Quantum Engineering, KAIST*
[b]*Department of Nuclear Engineering, Khalifa University of Science, Technology & Research (KUSTAR)*
[*]*Corresponding author: jeongiklee@kaist.ac.kr*

1. Introduction

The APR 1400 is a large pressurized water reactor (PWR). Just like many other water reactors, it has an emergency core cooling system (ECCS). One of the most important components in the ECCS is the safety injection tank (SIT). Inside the SIT, a fluidic device is installed, which passively controls the mass flow of the safety injection and eliminates the need for low pressure safety injection pumps. As more passive safety mechanisms are being pursued, it has become more important to understand flow structure and the loss mechanism within the fluidic device. Current computational fluid dynamics (CFD) calculations have had limited success in predicting the fluid flow accurately. This study proposes to find a more exact result using CFD and more realistic modeling.

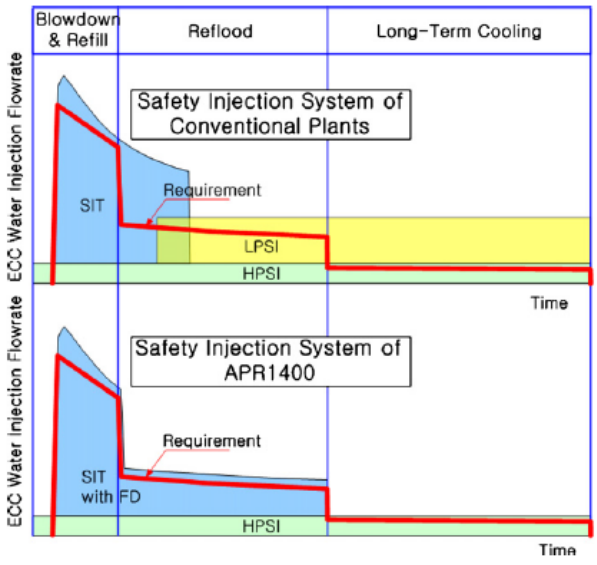

Fig. 1. Mass flow of SITs with and without fluidic devices [1]

2. CFD Analysis

CFD calculation is required in order to acquire the loss coefficient. However, numerically the problem is challenging since compressible fluid and incompressible fluid exist in the same large physical problem domain. To perform accurate simulation with realistic models, computation time may take months to years using a standard workstation. [2] Therefore the problem domain was confined to the fluidic device and discharge pipe for the preliminary calculation.

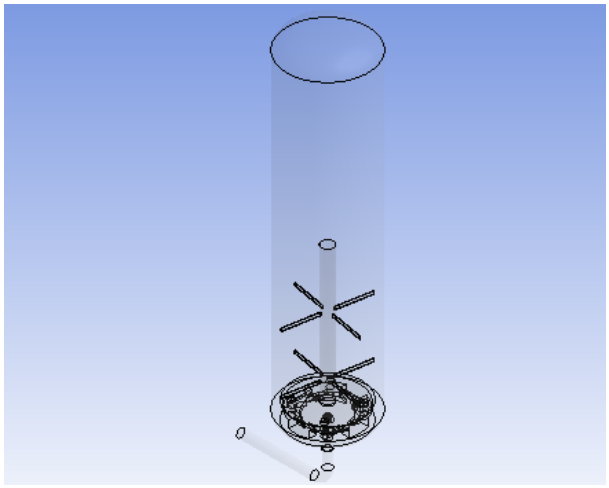

Fig. 2. SIT Geometry

Meshes were created using Ansys 14.0 Workbench while CFX was used for calculation. The k-epsilon model was chosen for the turbulence model. Mass velocity was given as the inlet boundary condition and atmospheric pressure was given as the outlet condition.

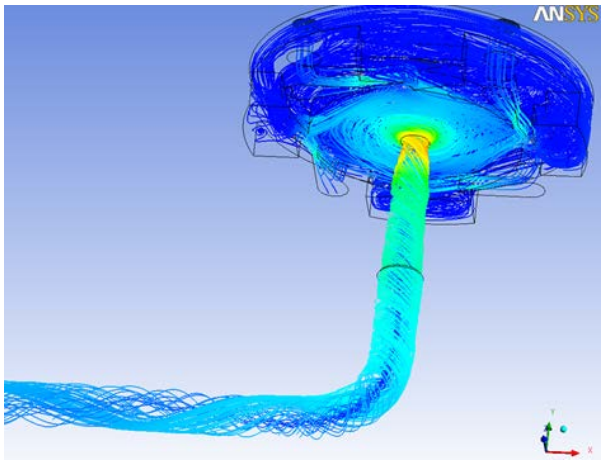

Fig. 3. 3D CFD results of streamline in discharge pipe

Experimental results were compared to those from CFD analysis. The total loss coefficients were calculated from the experiments and CFD simulation and compared in Fig. 4. It is noted that the time scale

and y-axis values are intentionally deleted to protect the proprietary data.

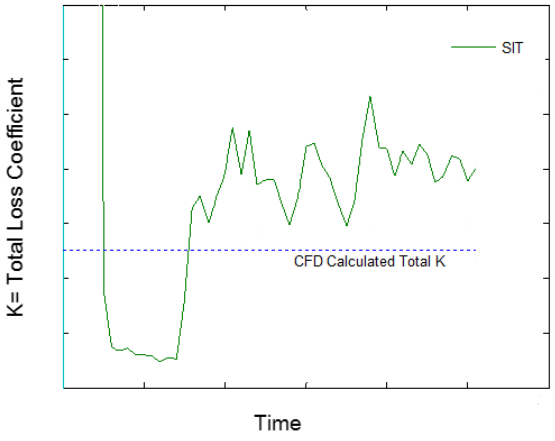

Fig. 4. Calculation of form loss coefficient from experimental results and CFD results

As we can see, calculations using CFD results deviate far from the actual phenomena. Therefore, more realistic modeling is necessary to describe a complex problem like this. The free-surface effect and nitrogen entrainment are two main effects that should be considered to improve calculations.

The K-epsilon model was used again for the detailed computation. Over 60,000 polyhedral meshes was used with a base size of 20cm. Due to the violent vortex, finer meshes with a base size of 2cm was needed in the fluidic device. The calculation was run under multiphase condition to simulate the nitrogen behavior. The tank was given a constant thermal resistance and constant ambient temperature with convective boundary condition on the tank wall. Lastly, a pressure boundary of 1 bar was given at the end of the discharge pipe. The successful transition from high flow to low flow can be seen in Fig. 5. More detailed CFD calculations will be provided in the conference presentation.

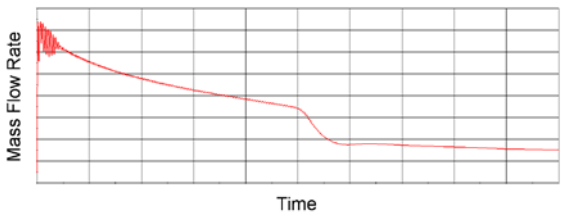

Fig. 5. Mass Flow Rate result from CFD

3. MARS Analysis

A thermal hydraulic system analysis code named MARS was used to check the validity. Two different approaches were used. The first uses the accumulator model that is implemented in the code itself. The other one uses pipes and junctions to model the tank. The pipe model is nodalized as in Fig. 6. Loss coefficients obtained from the vendor and the CFD calculation were used.

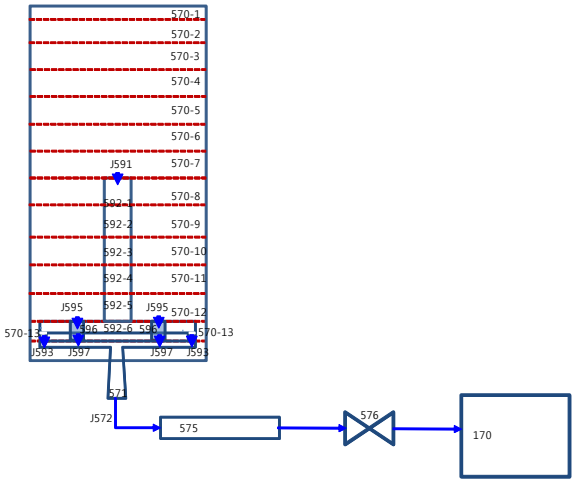

Fig. 6. Nodalization using pipes

3.1. Accumulator model

The experiment data was first compared with the accumulator model. Two valves were connected to the accumulator volume. Only one valve was open in the beginning. When the water level dropped below the stand pipe height, the valve was closed and the second valve was opened. Each valve had different form loss factors to control the mass flow. The form loss factors provided by the vendor was used. The result from the accumulator model fitted the experiment data incredibly well.

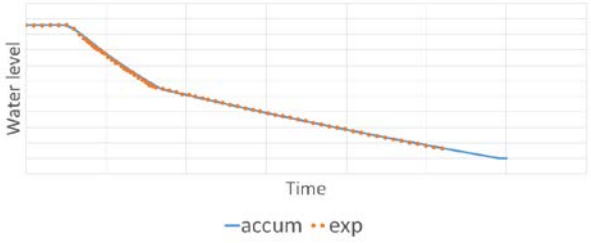

Fig. 7. Water level comparison of MARS accumulator model with experiment data

3.2. Pipe model

The pipe model uses pipes and junctions to describe the standpipe and fluidic device. In the accumulator model, we controlled the form loss factor in the discharge pipe. However, in this model we can give different form loss factors for the standpipe and fluidic device. By controlling the form loss factor, the water level curve was fit as close as possible. Since the high flow mode requires form loss factors from both the

standpipe and the fluidic device, the form loss factor of the fluidic device was determined first to fit the low flow mode. After that, the form loss factor of the standpipe was determined to fit the high flow mode. However the result was very counterintuitive. The form loss factor of the standpipe was about 6 times higher than the fluidic device. (Fig. 8.)

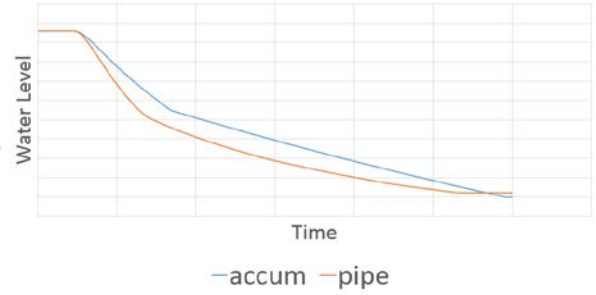

Fig. 8. Water level comparison of MARS accumulator model with pipe model

The mass flow rate in the standpipe and fluidic device were calculated. Initially, the mass flow rate was 0 kg/s for a few seconds. During the high flow, 30% of the water flowed through the standpipe. Then the mass flow through the standpipe became close to 0 kg/s when the water level dropped below the standpipe height.

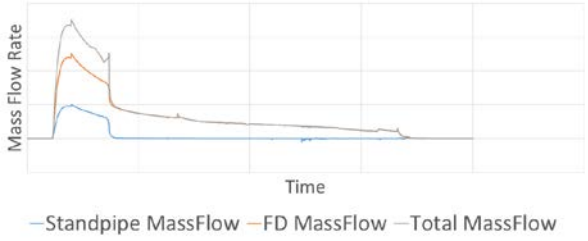

Fig. 9. Mass flow rate in standpipe and fluidic device

The water level from the bottom up to standpipe height is used to compare the water level inside and outside the standpipe. Once the water level drops below the standpipe height, the water level inside the standpipe immediately drops to near zero level and remains so.

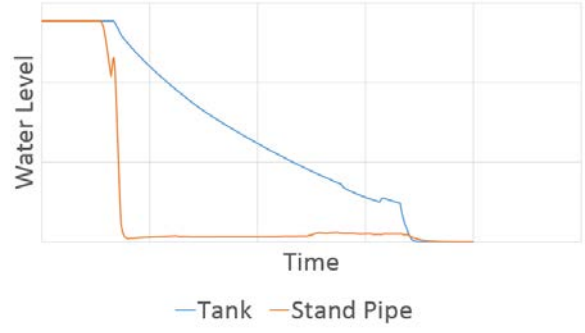

Fig. 10. Water level from bottom to standpipe height

The amount of nitrogen entrained through the discharge pipe can also be calculated. Once the water level inside the standpipe falls near zero, nitrogen starts to ingress into the core. The moment it starts to exit the tank, the mass flow peaks and then decreases over time. The total nitrogen entrained can be integrated over time and it adds up to more than 100 kg.

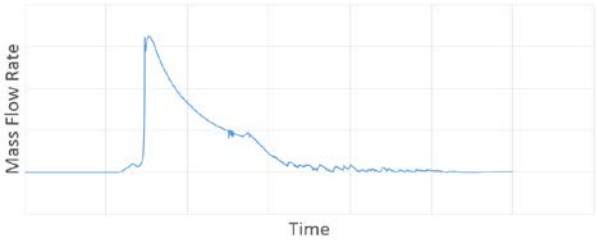

Fig. 11. Nitrogen mass flow rate

From Fig. 12, we can see that the accumulator model that uses the vendor specification matches the experimental results the best.

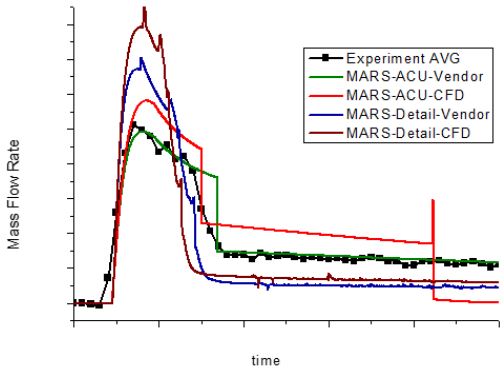

Fig. 12. Comparison of mass flow rates using different input models

4. Conclusions & Future Works

The SIT of APR1400 was analyzed using MARS and CFD. CFD calculation was executed first to obtain the form loss factor. Using the two form loss factors from the vendor and calculation, calculation using MARS was performed to compare with experiment. The accumulator model in MARS was quite accurate in predicting the water level. The pipe model showed some difference with the experimental data in the water level. Also, an unrealistically large amount of nitrogen entrainment was observed.

Once a detailed CFD computation is finished, a small-scale experiment will be conducted for the given conditions. Using the experimental results and the CFD model, physical models can be improved to fit the

results more accurately. The data from CFD and experiments will provide a more accurate k-factor which can later be applied in the MARS input using trips and multiple valves. Finally, the fluidic device design can be optimized for the future SIT designs.

ACKNOWLEDGMENTS

This research was supported by the KUSTAR-KAIST Institute, KAIST, Korea

REFERENCES

[1] I. C. CHU et al., Development of passive flow controlling safety injection tank for APR1400, Nuclear Engineering and Design Vol.238, p.200-206, 2008.
[2] S. G. LIM et al., Benchmark and parametric study of a passive flow controller (fluidic device) for the development of optimal designs using a CFD code, Nuclear Engineering and Design Vol.240, p.1139-1150, 2010.